First inverse kinematics measurement of resonances in ^{7}Be(α, γ)^{11}C relevant to neutrino-driven wind nucleosynthesis using DRAGON

A. Psaltis,[1,2,*] A. A. Chen,[1,2] R. Longland,[3,4] D. S. Connolly,[5,†] C. R. Brune,[6] B. Davids,[5,7] J. Fallis,[8] R. Giri,[6]
U. Greife,[9] D. A. Hutcheon,[5] L. Kroll,[1,2] A. Lennarz,[5] J. Liang,[1,‡] M. Lovely,[9] M. Luo,[10] C. Marshall,[3,4,§]
S. N. Paneru,[6,∥] A. Parikh,[11] C. Ruiz,[5,12] A. C. Shotter,[13] and M. Williams[5,14]
[1]*Department of Physics and Astronomy, McMaster University, Hamilton, Ontario L8S 4M1, Canada*
[2]*The NuGrid Collaboration, https://nugrid.github.io/*
[3]*Department of Physics, North Carolina State University, Raleigh, North Carolina 27695, USA*
[4]*Triangle Universities Nuclear Laboratory, Duke University, Durham, North Carolina 27710, USA*
[5]*TRIUMF, 4004 Wesbrook Mall, Vancouver, British Columbia V6T 2A3, Canada*
[6]*Department of Physics and Astronomy, Ohio University, Athens, Ohio 45701, USA*
[7]*Department of Physics, Simon Fraser University, Burnaby, British Columbia V5A 1S6, Canada*
[8]*North Island College, 2300 Ryan Road, Courtenay, British Columbia V9N 8N6, Canada*
[9]*Department of Physics, Colorado School of Mines, Golden, Colorado 80401, USA*
[10]*Department of Physics and Astronomy, University of British Columbia, Vancouver, British Columbia V6T 1Z4, Canada*
[11]*Department de Física, Universitat Politècnica de Catalunya, E-08036 Barcelona, Spain*
[12]*Department of Physics and Astronomy, University of Victoria, Victoria, British Columbia V8W 2Y2, Canada*
[13]*School of Physics, University of Edinburgh EH9 3JZ Edinburgh, United Kingdom*
[14]*Department of Physics, University of York, Heslington, York YO10 5DD, United Kingdom*

(Received 31 December 2021; revised 1 July 2022; accepted 12 September 2022; published 14 October 2022)

A possible mechanism to explain the origin of the light p nuclei in the Galaxy is the nucleosynthesis in the proton-rich neutrino-driven wind ejecta of core-collapse supernovas via the νp process. However, this production scenario is very sensitive to the underlying supernova dynamics and the nuclear physics input. As far as the nuclear uncertainties are concerned, the breakout from the pp chains via the ^{7}Be(α, γ)^{11}C reaction has been identified as an important link which can influence the nuclear flow and, therefore, the efficiency of the νp process. However, its reaction rate is poorly known over the relevant temperature range, $T = 1.5$–3 GK. We report on the first direct measurement of two resonances of the ^{7}Be(α, γ)^{11}C reaction with previously unknown strengths using an intense radioactive ^{7}Be beam from the Isotope Separator and Accelerator (ISAC-I) Center facility and the DRAGON recoil separator in inverse kinematics. We have decreased the ^{7}Be(α, γ)^{11}C reaction rate uncertainty to ≈9.4–10.7% over the relevant temperature region.

DOI: 10.1103/PhysRevC.106.045805

I. INTRODUCTION

The origin of the roughly 35 neutron-deficient stable isotopes with masses $A \geqslant 74$—between ^{74}Se and ^{196}Hg—in the proton-rich side of the valley of stability, known as the "p nuclei" is a long-standing puzzle in nuclear astrophysics [1–3]. The p nuclei were also traditionally referred to as "excluded" nuclei, since they were "shielded" by the s- and the r-process reaction paths [4]. For this reason their observed solar abundances [5], are 1 to 2 orders of magnitude smaller than their s- and r-process counterparts in the same mass region. It is generally accepted that the p nuclei in the solar system have been produced by more than one process; however, their synthesis mechanism is commonly referred to as the "p process."

The photodisintegration of preexisting neutron-rich seeds, which is one of the most promising nucleosynthesis scenarios of p-nuclei synthesis and is thought to take place in the oxygen neon layer of core-collapse supernovae, cannot reproduce the solar abundances of the light ^{92,94}Mo and ^{96,98}Ru isotopes, as well as the rare species ^{113}In, ^{115}Sn, and ^{138}La. Additional astrophysical sites/nucleosynthesis scenarios have been proposed, such as the thermonuclear explosions of Chandrasekhar mass carbon-oxygen white dwarfs [6], which is also supported by galactic chemical evolution models and the rp process in type-I x-ray bursts [7]. It is remarkable that despite the variety of astrophysical models, all these processes

---

[*] Present address: Institut für Kernphysik, Technische Universität Darmstadt, 64289 Darmstadt, Germany; psaltisa@mcmaster.ca

[†] Present address: Los Alamos National Laboratory, Los Alamos, New Mexico 87545, USA.

[‡] Present address: TRIUMF, 4004 Wesbrook Mall, Vancouver, British Columbia V6T 2A3, Canada.

[§] Present address: Department of Physics and Astronomy, Ohio University, Athens, Ohio 45701, USA.

[∥] Facility for Rare Isotope Beams, East Lansing, Michigan 48824, USA.

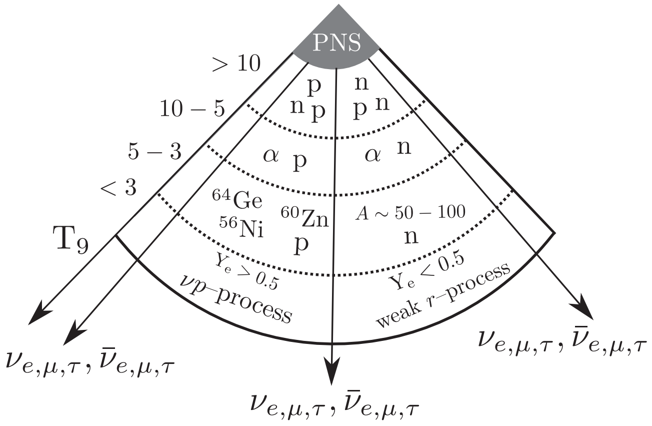

FIG. 1. Simplified schematic of the nucleosynthesis in neutrino-driven wind ejecta. The different stages and outcomes (νp process and weak r process) are shown. The figure is adapted from José and Iliadis [21].

can reproduce the solar abundances of most of the p nuclei to within a factor of 3 e.g., see the sensitivity studies in Refs. [8,9].

The advancement of multidimensional core-collapse supernova simulations with sophisticated neutrino transport methods, see Refs. [10,11] for the first studies that discussed this and Refs. [12,13] for some more recent results, suggests that the composition of the early innermost ejecta of the neutrino-driven wind that drives the explosion are mostly proton rich (the electron fraction Y_e is greater than 0.5)[1] [15,16] and that gives rise to a new nucleosynthesis scenario, the νp process [17–19], which can produce the lighter of the p nuclei.

To summarize the νp process, the neutrino-driven wind ejects very hot ($T > 10$ GK) and proton-rich material from the protoneutron star (see Fig. 1). At these extreme temperatures, the ejecta consist mainly of nucleons from dissociated nuclei. As the wind expands and cools down, nuclear statistical equilibrium assembles these nucleons into mainly ^{56}Ni and α particles (which are synthesised via the hot pp-chain sequence [20]) with an excess of free protons. At $T < 3$ to 4 GK, ^{56}Ni can rapidly capture free protons. However, the reaction flow cannot move beyond ^{64}Ge, which has a relatively long β^+ half-life of 1.06 min. This issue is resolved by electron antineutrino captures on free protons via the $p(\bar{\nu}_e, e^+)n$ reaction, which produce a small amount of free neutrons, 10^{-11}–10^{-12} of the total mass. At temperature drops from 3 to 1.5 GK, the much faster (n, p) reaction on ^{56}Ni, followed by a sequence of radiative proton captures, i.e., (p, γ) reactions, and further (n, p) reactions bypass ^{64}Ge and similar waiting points, such as ^{68}Se and ^{72}Kr with half-lives of 35.5 and 17.1 s, respectively. The reaction flow follows the $Z = N$ line up to the molybdenum region and then moves into more neutron-rich isotopes ($Z < N$) between molybdenum and tin. Finally, as the temperature drops below $T < 1.5$ GK, (p, γ) reactions freeze-out due to the Coulomb barrier, and the produced nuclei decay back to stability with ^{56}Ni still being the most abundant nucleus in the plasma.

The uncertainties of νp-process nucleosynthesis, mainly attributed to the supernova dynamics and the underlying nuclear physics input, have been explored by many groups [14,22–26] since it was first proposed. The most crucial component for a successful νp process is the electron fraction Y_e of the ejecta. Recent hydrodynamical studies with proper neutrino transport have shown that Y_e can lie between 0.5 and 0.6 before the onset of νp processing at $T = 3$ GK. Sensitivity studies have explored a variety of Y_e values, ranging from 0.5 to 0.8, and suggest that a higher Y_e leads to a more efficient νp process (i.e., production of heavier nuclei).

Concerning the nuclear physics input of the νp process the main uncertainties arise from a handful of reactions and the nuclear masses along the reaction path. The two most important reactions that dominate the nucleosynthesis in this scenario are the bottleneck $^{56}\mathrm{Ni}(n, p)^{56}\mathrm{Co}$ and triple-α—$^{4}\mathrm{He}(\alpha\alpha, \gamma)^{12}\mathrm{C}$—reactions. The former is always the first step of the νp process, and as a result controls the reaction flow with a smaller rate yielding a more efficient nucleosynthesis since the free neutrons synthesized from neutrino captures are captured by nuclei with $30 \leqslant Z \leqslant 42$, acting as “neutron poisons.”

The triple-α reaction controls the production of α particles, protons, and the ^{56}Ni seed before the onset and during the νp process. Therefore, it controls completely the neutron-to-seed ratio Δ_n as defined by Pruet *et al.* [19]. Our current knowledge of this reaction, despite its importance, is still limited and bears large experimental uncertainties. The three rates that are most commonly used in nucleosynthesis studies are those from Refs. [27–29]. In addition, Jin *et al.* [30] recently showed that an enhanced triple-α reaction due to an in-medium width change of the Hoyle state, suppresses the production of p nuclei in the νp process.

In the sensitivity study of Wanajo *et al.* [22], some alternative pathways were explored. In particular, the authors found that there are a couple of two-body reaction sequences, namely, $^{7}\mathrm{Be}(\alpha, \gamma)^{11}\mathrm{C}(\alpha, p)^{14}\mathrm{N}$ and $^{7}\mathrm{Be}(\alpha, p)^{10}\mathrm{B}(\alpha, p)^{13}\mathrm{C}$, which compete with the triple-α reaction, the main link between the pp-chain ($A < 12$) and CNO ($A \geqslant 20$) region, at the relevant temperature region $T = 1.5$–3 GK. This competition affects the Δ_n factor, and as a result, the reaction flow and the final elemental abundances. The authors studied the sensitivity of the final abundances by multiplying and dividing the $^{7}\mathrm{Be}(\alpha, \gamma)^{11}\mathrm{C}$ reaction rate by factors of 2 and 10. This rate variation affected the production of light p nuclei with $90 < A < 110$ up to an order of magnitude. A faster $^{7}\mathrm{Be}(\alpha, \gamma)^{11}\mathrm{C}$ rate leads to increased production of intermediate-mass nuclei that remove protons from the environment, acting as “proton poisons.” Subsequent studies, such as that by Nishimura *et al.* [26], also acknowledge the importance of the $^{7}\mathrm{Be}(\alpha, \gamma)^{11}\mathrm{C}$ reaction but do not provide a quantitative impact in the production of p nuclei. As we will discuss in detail in Sec. II, the $^{7}\mathrm{Be}(\alpha, \gamma)^{11}\mathrm{C}$ reaction rate is not well known in the relevant

---

[1] A relatively neutron-rich neutrino-driven wind ($0.4 < Y_e < 0.5$), leads to a different nucleosynthesis scenario called the weak r process, which can produce the lighter heavy elements with $Z = 26$–47 [14].

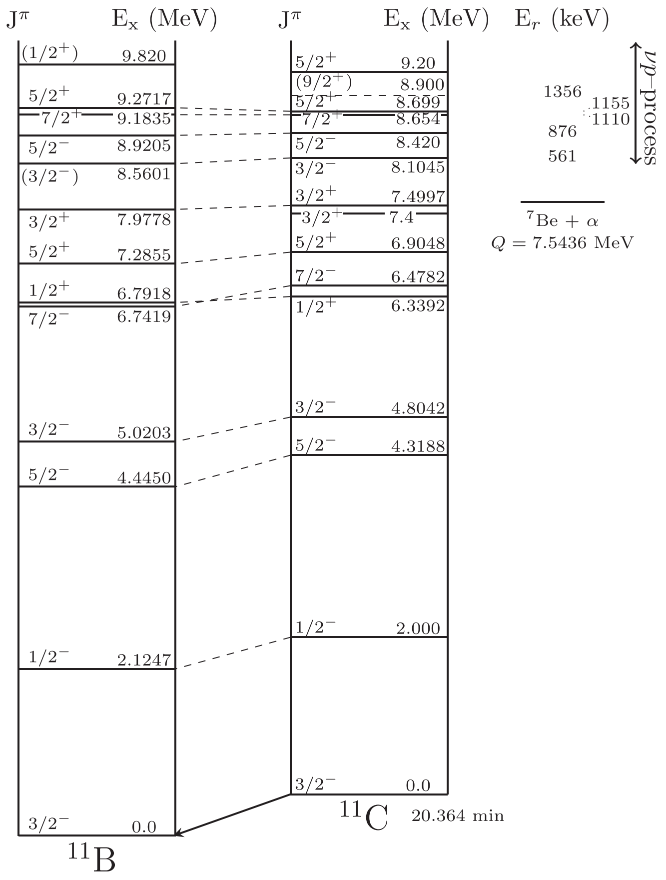

FIG. 2. Partial level scheme of the mirror nuclei ^{11}C and ^{11}B adopted from Kelley *et al.* [34] with the addition of the $E_x = 8.900$-MeV state from Yamaguchi *et al.* [33]. The dashed lines indicate isobaric analog states, and next to the ^{11}C scheme we present the α separation energy Q_α, the resonances of the ^{7}Be$(\alpha,\gamma)^{11}$C reaction E_r in keV and the relevant energy region for νp-process nucleosynthesis.

temperature range due to unknown resonance strengths, and, thus, an experimental study is required.

In the present paper we report on the first inverse kinematics study of the ^{7}Be$(\alpha,\gamma)^{11}$C reaction, using the DRAGON recoil separator and an intense ^{7}Be radioactive ion beam from the Isotope Separator and Accelerator (ISAC). The paper is structured as follows: in Sec. II we discuss the previous measurements regarding resonances of the ^{7}Be$(\alpha,\gamma)^{11}$C reaction. In Secs. III and IV we present the experimental details of the present paper along with the analysis procedures, and finally we discuss our results and conclusions in Secs. V and VI.

II. PREVIOUS MEASUREMENTS

Our current understanding of the ^{7}Be$(\alpha,\gamma)^{11}$C reaction over the energy region relevant to νp-process nucleosynthesis is based on three experimental studies [31–33].

Figure 2 shows the current level structure of ^{11}C along with its mirror ^{11}B, and in Table I we summarize the resonance parameters for the ^{7}Be$(\alpha,\gamma)^{11}$C reaction from the $A = 11$ evaluation of Kelley *et al.* [34].

The two lowest-lying energy resonances of the ^{7}Be$(\alpha,\gamma)^{11}$C reaction, which correspond to the $E_x = 8.105$ and 8.420 MeV levels in ^{11}C, were studied by Hardie *et al.* [31] in forward kinematics at Argonne National Laboratory. The authors used two methods to calculate the resonance strengths: The first was the thick target yield formula (similar to Eq. (4), and the second was a complementary relative method which employed the presence of ^{7}Li in the target, and the fact that they were studying the ^{7}Li$(\alpha,\gamma)^{11}$B reaction in the same campaign. More specifically, the relative method provided the resonance strength ratio between the resonances of interest in ^{7}Be$(\alpha,\gamma)^{11}$C and the known 660 keV ($E_x =$ 9.272 MeV in ^{11}B) resonance of the ^{7}Li$(\alpha,\gamma)^{11}$B reaction, reported in the same work. The main advantage of this method is that both the ^{7}Li:^{7}Be ratio in the target and the detector efficiencies are more accurately known than the number of ^{7}Be atoms alone and the absolute efficiencies. Nevertheless, one has to include an extra uncertainty factor from the ^{7}Li$(\alpha,\gamma)^{11}$B resonance. The adopted values for the two resonance strengths in Table I are the weighted averages of the two methods.

TABLE I. Resonance parameters for the ^{7}Be$(\alpha,\gamma)^{11}$C reaction from Kelley *et al.* [34]. The parameters for the resonance noted with a ⋄ are adopted from Yamaguchi *et al.* [33]. Tentative assignments and estimates are presented in parentheses. The resonances noted with a † were studied in the present paper. Values noted with a ‖ were adopted from the mirror nucleus ^{11}B. The proton partial widths Γ_p have been calculated using $C^2S = 1$.

E_x (MeV)	E_r (keV)	J^π	Γ_α	Γ_γ	Γ_p	ℓ	$\omega\gamma$ (eV)
7.4997(15)	−43.9(15)	$3/2^+$	2.2(1.6) eV	1.15 eV$^\|$		1	…
8.1045(17)	560.5(17)	$3/2^-$	6^{+12}_{-6} eV	0.350(56) eV		0	0.331(41)
8.420(2)†	876(2)	$5/2^+$	12.6(38) eV	3.1(13) eV		2	3.80(57)
8.654(4)†	1110(4)	$7/2^+$	$\leqslant$5 keV			3	…
8.699(2)†	1155(2)	$5/2^+$	15(1) keV	1.15(16) eV$^\|$		1	…
8.900⋄	1356	$(9/2^+)$	$>$8 keV			(3)	(1.2)
9.645(50)	2101(50)	$(3/2^-)$	210(40) keV	17 eV$^\|$	48(9) eV	0	…
9.780(50)	2236(50)	$(5/2^-)$	240(50) keV	1 eV$^\|$	520(100) eV	2	…
9.970(50)	2426(50)	$(7/2^-)$	120(20) keV	1 eV$^\|$	760(140) eV	2	…
10.083(5)	2539(5)	$9/2^+$	≈230 keV	$<$0.2 eV$^|$	900(180) eV	3	…

Wiescher *et al.* [32] studied the $E_x = 8.654$ and 8.699 MeV levels in ^{11}C, which correspond to the 1110 and 1155 keV[2] resonances of the $^7\mathrm{Be}(\alpha,\gamma)^{11}\mathrm{C}$ reaction. They used the $^{10}\mathrm{B}(p,\gamma)^{11}\mathrm{C}$ reaction in forward kinematics employing three different linear accelerators, covering a wide energy range ($E_x = 8 - 10.7$ MeV). In all three experimental setups, several detectors were used, allowing for angular distribution measurements. The authors observed primary γ transitions from the $E_x = 8.654$ and 8.699 MeV states and calculated the ratio Γ_γ/Γ for them using the cross sections from the γ-ray and α-particle channels, $\sigma(p,\gamma)/\sigma(p,\alpha)$. The most recent study relevant to the $^7\mathrm{Be}(\alpha,\gamma)^{11}\mathrm{C}$ reaction was performed by Yamaguchi *et al.* [33] using the low-energy radioactive ion beam facility CRIB [35] at the Center for Brain Science in RIKEN, Japan. The $^7\mathrm{Be}+\alpha$ resonant scattering and $^7\mathrm{Be}(\alpha,p)$ reaction measurements were performed using the thick-target method in inverse kinematics and provided the excitation functions for $E_x = 8.7$–13.0 MeV. The R-matrix analysis of the data shows two small peaks in the low-energy region, between 8.90 and 9.20 MeV. The first one is considered to be the known $5/2^+$ state at 9.20 MeV observed by Wiescher *et al.* [32]. The second one, located at around 8.90 MeV, is regarded by the authors as a new resonance. However, they argue that this spectral feature could also originate from either the $E_x = 8.655$ or the 8.699 MeV states since their the energy uncertainty was quite large in this energy region. Finally, all this information about the $^7\mathrm{Be}(\alpha,\gamma)^{11}\mathrm{C}$ resonances is summarized in Table I.

The current $^7\mathrm{Be}(\alpha,\gamma)^{11}\mathrm{C}$ reaction rate is based on a calculation from NACRE (I and II) [28,36] and includes contributions only from the 561 and 876 keV resonances for which experimentally measured strengths exist, and the nonresonant (DC) contribution is adopted with the same parameters as those of the mirror $^7\mathrm{Li}(\alpha,\gamma)^{11}\mathrm{B}$ reaction for $T < 0.7$ GK. Contributions from the broad resonances at 2101, 2236, 2426, and 2539 keV were also included in NACRE-II and affect the reaction rate for $T > 2$ GK. In NACRE-I the same high-energy part of the reaction rate was estimated using Hauser-Feshbach calculations. The rate that was used in the sensitivity study by Wanajo *et al.* [22] was the one from Angulo *et al.* [28] (NACRE-I), which is uncertain by factors of 1.87–2.54 in the relevant temperature region. The NACRE-II reaction rate is uncertain by factors of 1.76–1.91 for $T = 1.53$ GK. The uncertainties are derived from their potential model (PM), which is used to reproduce the experimental astrophysical S-factor data. $S(E) \equiv (E/e^{-2\pi\eta})\sigma(E)$, where E is the center-of-mass energy, and η is the Sommerfeld parameter, which is related to the charges and velocities of the interacting particles. More specifically, the uncertainties are calculated by using the maximum and minimum parameters of the PM. It is also worth noting that the subthreshold resonance at $E_x = 7.50$ MeV ($E_r = -43.9$ keV) has a large contribution at low temperatures, below $T \approx 0.3$ GK and according to Descouvemont [37], it could affect the production of ^{7}Li (fed by the decay of ^{7}Be) in classical novae [38].

TABLE II. Beam and gas target properties for the two independent measurements of the present paper.[a]

	E_{beam} (A keV)	E_{lab} (MeV)	I_{beam} $\times 10^8$ (s^{-1})	P_{target} (Torr)
Run 1	464.2(3)	3.249(2)	1.33(7)	7.9(1)
Run 1	442.7(2)	3.099(1)	2.06(8)	5.06(6)
Run 2	441.8(2)	3.093(1)	5.83(2)	4.89(3)
Run 2	351.8(3)	2.463(2)	3.45(12)	5.75(4)

[a] The 1110-keV resonance was studied in two independent measurements due to a low recoil yield in the first measurement.

III. EXPERIMENTAL DETAILS

The measurements of this paper were carried out using the DRAGON recoil separator [39] at TRIUMF, Canada's particle accelerator centre in Vancouver, BC. Intense beams of $^7\mathrm{Be}^+$ were produced using the ISOL technique by bombarding thick ZrC and graphite targets with 55-μA 500-MeV protons from the TRIUMF cyclotron. The $A=$ 7 isobars, mainly ^{7}Li and ^{7}Be, were extracted from the target through a high-resolution mass separator, and the beryllium ionization was enhanced using the TRIUMF Resonant Ionization Laser Ion Source [40]. After the ion source, the beam was transported through the ISAC high-resolution ($M/\Delta M = 2000$) mass separator and then accelerated through the ISAC-I radiofrequency quadrupole and drift-tube linac (DTL) to energies so that each resonance was centered in the gas target (see Table II for details). The beam energies were chosen in order to cover center-of-mass windows of 1157 ± 24, 1111 ± 13, and 878 ± 17 keV, across the gas target volume. To ensure a pure contaminant-free radioactive ion beam, an additional carbon stripping foil of 20 $\mu g/\mathrm{cm}^2$ was placed downstream of the DTL allowing fully stripped $^7\mathrm{Be}^{4+}$ to be selected using a bending magnet for transport to DRAGON, thus, eliminating the main isobaric contaminant ^{7}Li. This technique has also been used in other radioactive beam facilities [41]. Finally, $^7\mathrm{Be}^{4+}$ was delivered at the helium-filled windowless gas target of DRAGON at mean intensities of ≈ 1.3–5.8×10^8 pps (see Sec. IV C for normalization details of the intensities).

DRAGON has four main components: (a) the windowless differentially pumped recirculating gas target, (b) the γ-ray detector array, (c) the electromagnetic mass separator, and (d) the recoil detection system, which are shown in the schematic of Fig. 3.

The γ-ray array consists of 30 BGO scintillator crystals with photomultiplier tubes covering 89–92% of the 4π solid angle [42]. The segmented array allows for the detection of individual prompt γ rays from the radiative capture reactions inside the gas target and the tagging of the associated recoil particles, which provides an additional background reduction in the focal plane detectors.

The DRAGON electromagnetic mass separator consists of two magnetic (M) and two electric dipoles (E) in a MEME configuration. The two-stage separation begins with the first magnetic dipole (MD1), which selects a single charge stage to be transmitted through DRAGON. For our paper, we tuned DRAGON to the $q = 2^+$ charge state for all resonances.

---

[2] All resonance energies are expressed in the center-of-mass system.

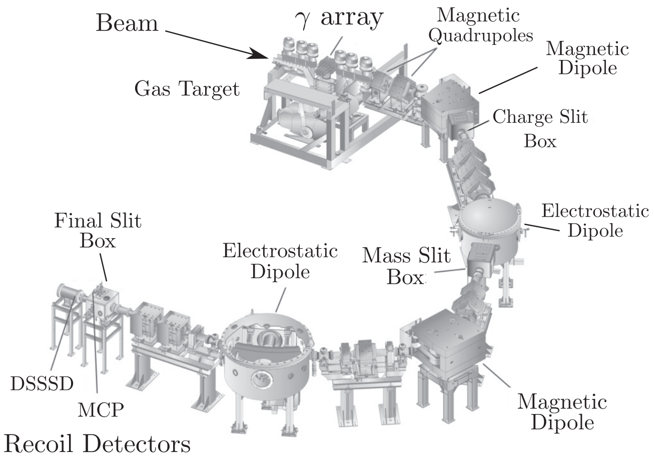

FIG. 3. Schematic of the DRAGON recoil separator. The main components are shown.

Recoils that do not have the aforementioned charge are deflected to slits that are located downstream of the MD1. Subsequently, the recoils are led to the first electric dipole (ED1) where they are separated according to mass. ED1 is followed by the second stage of magnetic and electric dipoles (MD2 and ED2) until the beam reaches the focal plane where the heavy-ion detectors are located.

Close to the focal plane of DRAGON we employed a microchannel plate (MCP) and a double-sided silicon-strip detector (DSSSD). The MCP provided the starting timing signal for a local time-of-flight (TOF) transmission measurement [43]. In the DSSSD, the recoils are stopped, their kinetic energy and position are measured, and the stopping timing signal is recorded. In addition, we employed the prompt γ rays from the BGO array as a starting signal for a "separator TOF" measurement for the coincidence analysis (see Sec. IV B). The data were recorded using a state-of-the-art time-stamp-based data acquisition system [44].

It is worth mentioning that such a measurement using DRAGON and any other recoil separator dedicated to resonance strength measurements is quite challenging due to geometric considerations. The maximum recoil angle of the reaction at the resonance energies of interest can be calculated using the following equation:

$$\theta_{r,\max} = \arctan\left(\frac{E+Q}{\sqrt{2m_1c^2\left(\frac{m_1+m_2}{m_2}\right)E}}\right), \tag{1}$$

where E is the center-of-mass energy, Q is the reaction Q value, and m_1, m_2 are the masses of the projectile and the target nuclei, respectively. This corresponds to a single γ-ray emission to the recoil nucleus ground state at 90° in the center-of-mass system.

For the $^7\text{Be}(\alpha,\gamma)^{11}\text{C}$ reaction maximum recoil angles are $\theta_{r,\max} = 42.67$ mrad for the 1155 keV, 43.3 mrad for the 1110 keV, and 47.42 mrad for the 876 keV. These numbers far exceed the nominal angular acceptance of DRAGON, $\theta_{\text{DRAGON}} = \pm 21$ mrad). For this reason, we performed detailed GEANT simulations of DRAGON [45,46] to extract the transmission of the recoils though the separator ($\eta_{\text{separator}}$), and in addition, the BGO array efficiency (η_{BGO}), which are used for the resonance strength calculations. References [42,47,48] provide an in-depth discussion about this approach, and in Sec. IV F we provide the specifics for the study of the $^7\text{Be}(\alpha,\gamma)^{11}\text{C}$ reaction.

IV. DATA ANALYSIS

We performed yield measurements for three beam energies, corresponding to the 1155, 1110, and 876 keV resonances of the $^7\text{Be}(\alpha,\gamma)^{11}\text{C}$ reaction (see Fig. 2). As we have already discussed in Sec. II, the 876-keV resonance strength has been measured by Hardie *et al.* [31], whereas the latter two resonances have unknown strengths. Our reasoning to remeasure that resonance is twofold: On one hand it is believed to have the greatest impact on the current reaction rate at νp-process energies [36], and on the other hand it will provide one additional demonstration that DRAGON can measure resonance strengths for reactions in which the angular spread of the recoils exceeds its nominal acceptance [47,48].

A. Thick target yield and resonance strength

The calculation of thermonuclear reaction rates in a laboratory setting requires the determination of the reaction cross section. Instead, what is actually measured in experimental studies is the reaction yield, which can be simply expressed as

$$Y = \frac{\mathcal{N}_{\mathcal{R}}}{\mathcal{N}_{\mathcal{B}}}, \tag{2}$$

where $\mathcal{N}_{\mathcal{R}}$ is the number of reactions that occur and $\mathcal{N}_{\mathcal{B}}$ is the number of incident beam particles. In fact, an experimental setup has a finite detection efficiency, in our case, η_{DRAGON}, meaning that it does not detect the total number of reactions but rather a fraction of it N_r. According to the analysis mode that we use, singles or coincidences (see Sec. IV B), η_{DRAGON} can be either $\eta_{\text{DRAGON}}^{\text{singles}} = \eta_{\text{separator}} f_q \eta_{\text{MCP}} \eta_{\text{DSSSD}} \eta_{\text{live}}^{\text{singles}}$, or $\eta_{\text{DRAGON}}^{\text{coinc}} = \eta_{\text{separator}} f_q \eta_{\text{BGO}} \eta_{\text{MCP}} \eta_{\text{DSSSD}} \eta_{\text{live}}^{\text{coinc}}$, respectively. The experimental yield is then given by

$$Y = \frac{\mathcal{N}_r}{\mathcal{N}_{\mathcal{B}} \eta_{\text{DRAGON}}}. \tag{3}$$

We can also express the energy-dependent reaction yield as a relation between the cross-section $\sigma(E)$ and the target thickness ΔE, or better, the stopping power of the target $\varepsilon(E)$, for beam energy E_{beam} using

$$Y(E_{\text{beam}}) = \int_{E-\Delta E}^{E} \frac{\sigma(E)}{\varepsilon(E)} dE. \tag{4}$$

For narrow resonances with constant stopping power over the resonance width, which can be found in reactions relevant for astrophysics, we can calculate the integral of Eq. (4) analytically using a single-level Breit-Wigner (Lorentzian) cross-section profile [49]. Specifically, in the case of an infinitely thick target, that is, $\Delta E \rightarrow \infty$, or, equivalently,

$\Delta E \gg \Gamma$, we have

$$Y(E_{\mathrm{beam}}) = \frac{\lambda_r^2}{2\pi}\frac{\omega\gamma}{\varepsilon_r}\left[\tan^{-1}\left(\frac{\mathrm{E}_{\mathrm{beam}} - E_r}{\Gamma/2}\right) + \frac{\pi}{2}\right], \tag{5}$$

where λ_r and ε_r are the de Broglie wavelength and the target stopping power in the center of the mass system, E_r is the energy of the resonance, Γ is its width, and ΔE is the target thickness. Solving for $E_{\mathrm{beam}} = E_r$, we can obtain a simple expression for the reaction yield and the resonance strength $\omega\gamma$,

$$\omega\gamma = \frac{2Y_{\Delta E\to\infty}\varepsilon}{\lambda_r^2}\frac{m_1}{m_1 + m_2}, \tag{6}$$

where the reaction yield $Y_{\Delta E\to\infty}$ is given by Eq. (3) and ε is the target stopping power in the laboratory frame—a discussion on how it is measured in DRAGON experiments can be found in Sec. IV E.

B. Particle identification

The first step towards determining the reaction yield and, subsequently, the strength of a resonance is the identification of the reaction products or recoils. For this, we employed two distinct methods: A detection of ^{11}C recoils in singles, using the DSSSD and a local TOF (MCP-DSSSD), and in γ-recoil coincidences using the separator TOF (BGO-DSSSD). Figure 4 shows typical particle identification plots for the three resonances of the ^{7}Be$(\alpha,\gamma)^{11}$C reaction both in singles (gray points) and in coincidences (colored points) with additional software cuts, such as the energy range of the γ rays in the BGO array and the energy deposited in the DSSSD, providing further recoil discrimination. It is evident that for the 876- and 1110-keV resonances the yield is low, but the signal is clear and without any unwanted background, such as the unreacted, "leaky" beam. This is consistent with the fact that DRAGON is able to reject unreacted beam particles from (α,γ) reactions very efficiently and has demonstrated a beam suppression of $>10^{13}$ [50]. In the present experiment, the rejection is higher due to the use of a fully stripped beam and the fact that the selected carbon recoils have a very different charge state (4^+ vs 2^+).

In addition to the aforementioned methods, we could also identify the recoils of interest using a timing signal of the 11.8-MHz ISAC-I radio-frequency (RF) quadrupole accelerator and the capture of a coincidence γ ray by the BGO array (BGO-RF) [39,44]. Figure 5 shows the results for each resonance.

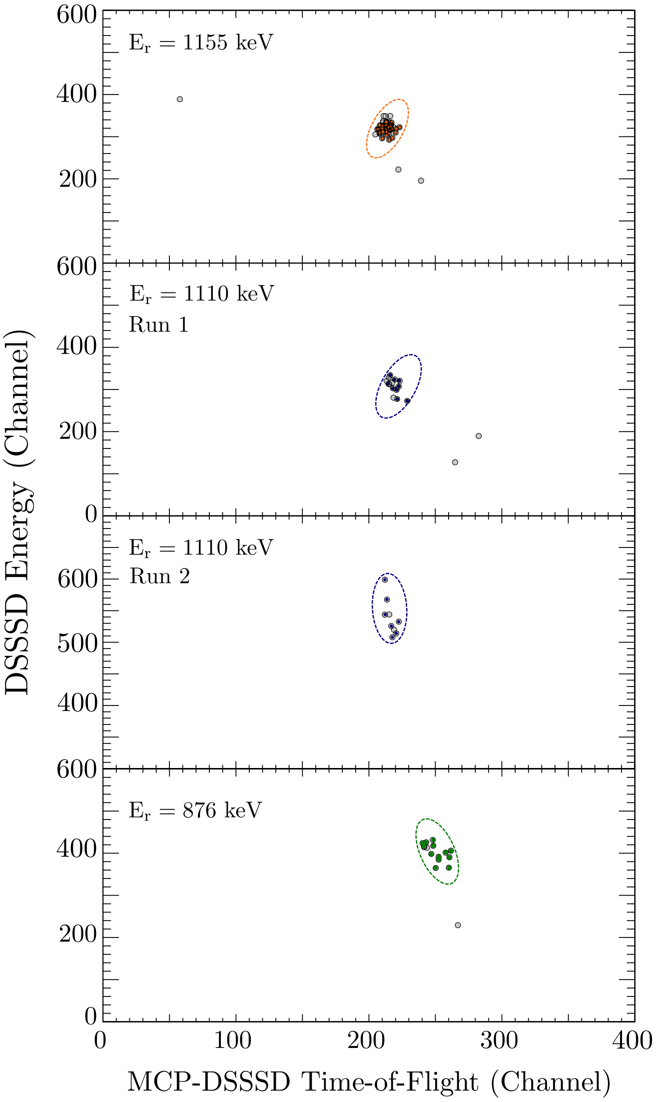

FIG. 4. Particle identification plot for the ^{11}C recoils for each of the resonances we studied in the present paper using the local time-of-flight transmission measurement and the energy deposited in the DSSSD at the focal plane of DRAGON. The colored and gray points correspond to coincident and singles recoils events, respectively. For the 1110 keV, we show the two independent measurements in separate panels. See the text for details.

C. Beam normalization

We monitored the ^{7}Be beam current throughout the experiment using silicon surface barrier detectors (SSB) at well-defined laboratory angles of 30° and 57° with respect to the beam axis by detecting the elastically scattered target particles. Due to the low count rate in the SSB detectors, we did not use SSB measurements for short time windows Δt, before and after each yield measurement to calculate the beam normalization $\mathcal{R}$ factor as is typical in DRAGON experiments (see, for example, the works in Refs. [39,51–53]). Instead, we first ensured that the beam current during each run was stable by checking the current on the charge slits after the first magnetic dipole and used the total integrated counts in the SSBs per yield run to calculate the $\mathcal{R}$ factor, which is given by

$$\mathcal{R} = \frac{I}{|qe|}\frac{\Delta t}{N_\alpha}\frac{P}{E_b^2}\eta_{\mathrm{target}}, \tag{7}$$

where I is the average current reading at the upstream Faraday cup before the gas target, q is the beam charge state (4^+), e is the elementary charge ($e = 1.6\times10^{-19}$ C), N_α is the number of scattered α particles detected by the surface barrier detectors during the yield run time Δt, P is the gas target

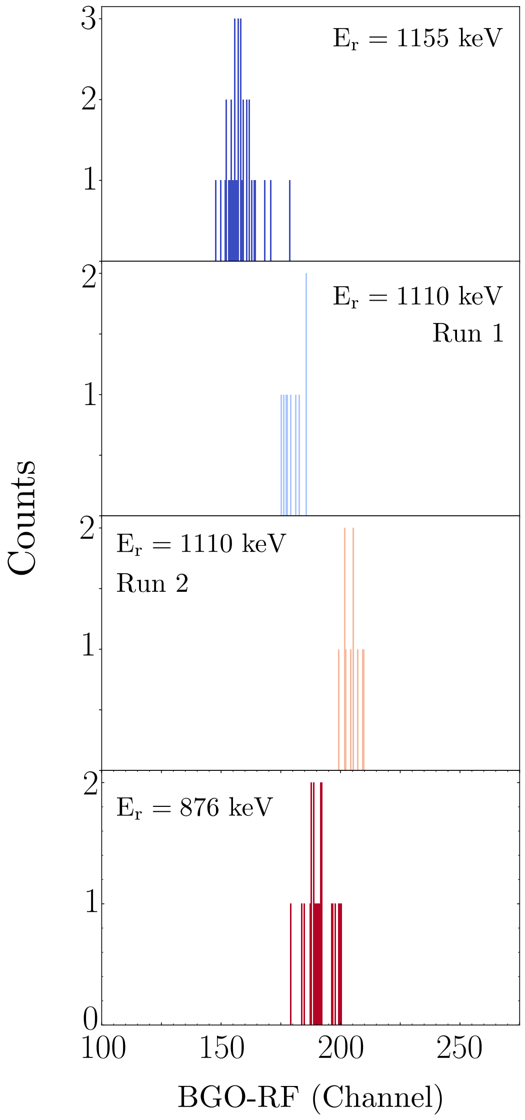

FIG. 5. Particle identification plot using the BGO vs accelerator RF time-of-flight for coincident recoil events. The RF period is $\tau_{\mathrm{RF}} = 84.8$ ns.

pressure in Torr, E_b is the beam energy in keV/u, and η_{target} is the transmission through an empty target. We assume only elastic Rutherford scattering for the target particles and the E_b^2/P factor enters Eq. (7) to make $\mathcal{R}$ invariant to the chosen beam energy and target pressure [54].

The normalized number of beam particles N_{beam} is then given by

$$N_{\mathrm{beam}} = \mathcal{R} N_\alpha \frac{E_b^2}{P}. \tag{8}$$

Table III shows the $\mathcal{R}$-factor results for all the yield measurements of the present paper. Note that in our two independent experimental runs we used different SSB gains, threshold settings, and prescalers. For this reason, the N_α that we use in Eqs. (7) and (8) to extract N_{beam} are also different.

TABLE III. Beam normalization results for the yield measurements of the present paper.[a]

	E_{beam} (A keV)	$\mathcal{R}$-factor (^{7}Be /α)(Torr/keV^2)	N_{beam} $\times 10^{13}$ ions
Run 1	464.2(3)	$1.15(2) \times 10^{11}$	1.07(2)
Run 1	442.6(2)	$1.22(2) \times 10^{11}$	1.76(5)
Run 2	441.8(2)	$1.74(4) \times 10^{10}$	1.53(4)
Run 2	351.8(3)	$2.77(6) \times 10^{10}$	2.12(4)

[a] During the two independent experimental runs, we used different SSB gains, threshold settings, and prescalers. For this reason the absolute value of the SSB rate is not comparable between these different periods.

D. Carbon in helium charge state distribution

DRAGON is tuned to select and transport a single charge state to the final focal plane. For this reason, an accurate knowledge of the recoil charge state distribution is necessary to determine the total reaction yield. Since the recoil nucleus, in our case ^{11}C is unstable, an abundant and stable isotope of the same element is used instead—^{12}C. The stable ion beam for this measurement was provided from the microwave ion source of the ISAC off-line ion source [55].

At DRAGON, the charge state distributions can be determined experimentally by measuring the beam current on Faraday cups before and after the gas target, and comparing it to the current on a Faraday cup downstream from the first magnetic dipole (see Fig. 3). We chose to tune DRAGON to the 2^+ charge state because according to theoretical calculations [56], it is the maximum of the distribution, thus, providing the highest recoil yield. Figure 6 shows the results for this charge charge for energies corresponding to the ^{7}Be$(\alpha,\gamma)^{11}$C resonance strengths.

E. ^{7}Be stopping power in ^{4}He

The stopping power ϵ of the gas target is an important component for the calculation of the reaction yield. The advantage

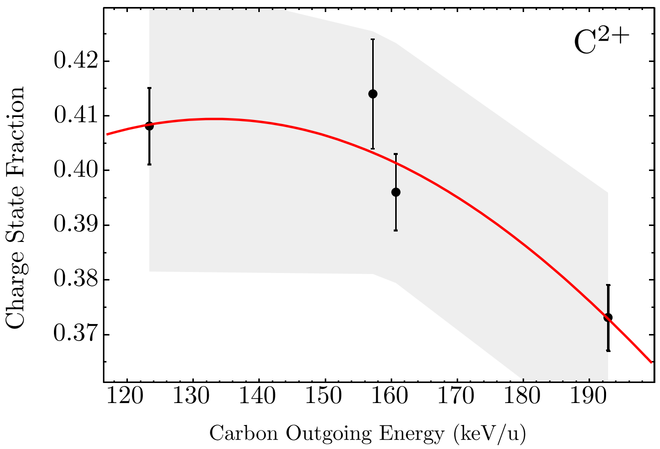

FIG. 6. Experimentally measured carbon in helium charge state distribution. The fit to the experimental data is a Gaussian function, and the band gives the 1σ-confidence interval to the fit.

TABLE IV. Summary of the ^{7}Be in ^{4}He stopping power measurements. The experimental results are compared with the calculations of SRIM [57]. The units of ϵ are eV/ (10^{15} atoms/cm^2).

E_{beam} (A keV)	ϵ_{DRAGON}	ϵ_{SRIM}
464.2(3)	40.7(15)	38.2
442.6(2)	39.7(15)	38.8
441.9(2)	39.5(15)	38.8
351.8(3)	41.5(18)	39.6

of recoil separators, such as DRAGON, is that the stopping power is measured directly and it is not based on semiempirical estimates that can introduce an additional uncertainty factor in the final result. At DRAGON, the stopping power is measured by varying both the pressure of the gas target, and the magnetic-field strength needed to center the beam at a momentum dispersed angular focus after the first magnetic dipole. Our experimental results agree to within 6% with calculations using the SRIM code [57] as shown in Table IV.

F. GEANT simulations of DRAGON

As we have already pointed out in the above, detailed simulations using GEANT are needed to determine the recoil transmission $\eta_{\text{separator}}$ and the efficiency of the BGO array η_{BGO}, which are used to calculate the reaction yield, and, subsequently, the resonance strength $\omega\gamma$ as part of the recoil detection efficiency of DRAGON η_{DRAGON}.

The DRAGON GEANT simulation toolkit[3] has been extensively used for experimental planning, such as in the study of the ^{12}C$(\alpha,\gamma)^{16}$O reaction [59], and its results show agreement with experimental data to within 1–10% [46].

The simulation input file includes all the information GEANT requires to perform the simulation, such as the energy, spin, lifetime, and γ-branching ratios for each nuclear level and the energy and width of the resonance of interest (see Table V for an overview). For the study of the ^{7}Be$(\alpha,\gamma)^{11}$C reaction, the nuclear information was adopted from the A=11 evaluation of Kelley *et al.* [34]. Specifically for the 1110-keV resonance since there are no experimentally measured γ-branching ratios, we adopted those of the mirror state in ^{11}B. For the γ-ray angular distribution $W(\theta)$, which affects both the transmission of the recoils and the BGO array efficiency [42,47], we calculated all the possible $W(\theta)$'s for each cascade, following the prescription of Rose and Brink [60]. In addition, we changed the gas target pressure in the simulation in order to obtain the same stopping power as in the experiment (see Sec. IV E).

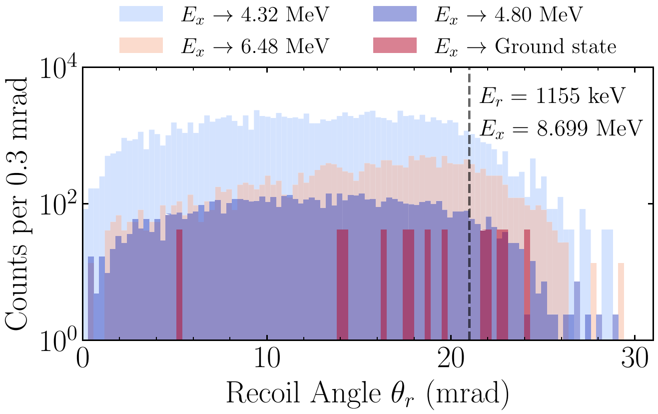

FIG. 7. Angular distribution for recoils of the E_r= 1155 keV resonance that hit the focal plane detector (DSSSD) using GEANT. The contributions from different cascades are shown. The vertical dashed line defines the angular acceptance of DRAGON, θ_{DRAGON} = 21 mrad.

We performed simulations for each resonance energy within its uncertainty, ±2, ±4, and ±2 keV for the 1155-, 1110-, and 876-keV resonance respectively. The final results used in the data analysis are the averages of these simulations and the systematic uncertainty is attributed mainly to the uncertainty in the γ-branching ratios and the range of possible γ-angular distributions.

Figure 7 shows the results from a simulation of the E_r = 1155 keV resonance. It is evident that transitions with a cascade of multiple γ rays, such as 8.699 → 4.32 MeV provide more favorable conditions for transmission through the separator since their recoil angular distribution from multiple decay vectors averages out with resulting maximum intensity at lower angles as Ruiz *et al.* [42] argue.

---

[3] The GEANT simulation package of DRAGON can be found in Ref. [58].

TABLE V. Settings of the GEANT simulation for the ^{7}Be$(\alpha,\gamma)^{11}$C data analysis. Nuclear properties were adopted from Kelley *et al.* [34]. For the 1110-keV resonance, the branching ratios of the mirror nucleus ^{11}B are used.

Quantity	E_r = 876 keV			E_r = 1110 keV			E_r = 1155 keV		
Excited-state lifetime	0.030 fs			1.31×10^{-19} s			4.3×10^{-20} s		
Resonance energy (keV)	874-878			1106–1114 keV			1153–1157 keV		
Particle (α) partial width	12.6 eV			5 keV			15 keV		
	E_x^i (MeV)	E_x^f (MeV)	B.R.s	E_x^i (MeV)	E_x^f (MeV)	B.R.s	E_x^i (MeV)	E_x^f (MeV)	B.R.s
γ branching ratios (B.R.s)	8.420	0	93	8.654	0	0.9 ± 0.3	8.699	0	42 ± 10
		4.319	7		4.319	86.6 ± 2.3		4.319	42 ± 10
					6.478	12.5 ± 1.1		4.804	2.4 ± 1.5
								6.478	13.6 ± 4.6

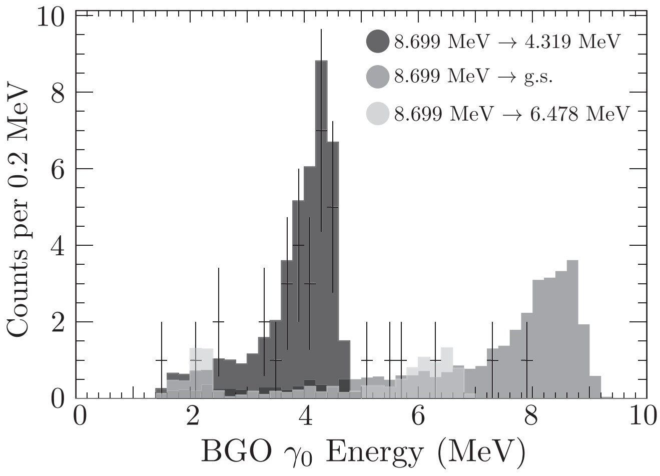

FIG. 8. Comparison between the experimental data (points) and the GEANT simulation (histograms) for a BGO γ_0-ray energy spectrum from the 1155 keV resonance. The two dominant γ transitions to the $E_x = 4.319$ MeV and the ground state can be clearly seen in the simulation results. We do not depict the weak transition to the $E_x = 4.804$ MeV state. See the text for details.

V. RESULTS

In the following, we will discuss the results from each resonance studied in the present paper and then present the uncertainties and the calculation of the new thermonuclear reaction rate $N_A\langle\sigma v\rangle$.

A. Strength of the 1155-keV resonance

For the highest-energy resonance we studied in the present paper, 1155 keV, we detected a strong, background-free signal as is evident in the particle identification (PID) plot of Fig. 4. Clusters of 33 and 49 recoil events in coincidence and singles modes were detected, despite the low recoil transmission through the separator [$\eta_{\text{separator}} = 0.141(28)$, see also Table VIII].

The GEANT simulations we performed for this resonance are in very good agreement with the experimental results as Fig. 8 shows (see also Fig. 2 of Ref. [61] for the same resonance). It is worth noting that DRAGON is more sensitive to the detection of recoils that γ decay to the $E_x = 4.319$-MeV state, compared to the ground state as we discussed in Sec. IV F.

The final result for the resonance strength is $\omega\gamma_{1155} = 1.73 \pm 0.25(\text{stat.}) \pm 0.40(\text{syst.})$ eV was adopted from the singles analysis and had a smaller uncertainty compared to the coincidence analysis result. However, the two results are in agreement (see also Table VI).

B. Strength of the 1110-keV resonance

The 1110-keV resonance was studied in two independent experimental runs due to the low recoil yields. We detected $14^{+4.3}_{-3.7}$ and $9^{+3.8}_{-2.7}$ events in singles with different integrated beam fluxes $1.76(5) \times 10^{13}$ and $1.53(5) \times 10^{13}$ ions, respectively (see also Table III). The asymmetric uncertainty in the amount of detected recoils was calculated according to the prescription of Feldman and Cousins [62] for a Poissonian signal with zero background as we can see from the PID plots of Fig. 4.

To account for the asymmetric uncertainties and provide a realistic statistical uncertainty for the number of detected ^{11}C recoils, we proceeded as follows: We first used Fechner's two-piece normal distribution [63] for the two independent runs, using the Feldman and Cousins [62] prescription for the variances (see Fig. 9, top). After that, we created a combined probability distribution by calculating averages by randomly sampling from the two individual distributions. The final results for the detected ^{11}C recoils and their respected 1 and 2σ uncertainties are then calculated from the combined distribution. We find $12.1^{+2.7}_{-2.5}$ (1σ) and $^{+5.3}_{-4.8}$ (2σ) events for the 1110-keV resonance in singles, corresponding to $^{+22.3}_{-20.7}\%$ (1σ) and $^{+43.8}_{-39.7}\%(2\sigma)$ statistical uncertainty, respectively, as we show in in Fig. 9.

The resonance strengths resulting from singles and coincidence analysis are $\omega\gamma_{1110,\text{singles}} = 125^{+27}_{-25}(\text{stat.}) \pm 15(\text{syst.})$ MeV and $\omega\gamma_{1110,\text{coinc}} = 161^{+43}_{-41}(\text{stat.}) \pm 24(\text{syst.})$ MeV, respectively, from which we choose the former as the final result. The large difference compared to the 1155-keV resonance strength—almost an order of magnitude—can be attributed to the difference in the orbital angular momentum $\ell_\alpha = 1$ for the former state and $\ell_\alpha = 2$ for the latter (see Table I).

C. Strength of the 876-keV resonance

For the lowest energy in this paper, the maximum recoil angle is $\theta_{r,\text{max}}$= 47 mrad, which is the largest ever attempted

TABLE VI. Resonance strengths $\omega\gamma$ of the ^{7}Be$(\alpha,\gamma)^{11}$C reaction resonances from the literature [31,34] and the present paper (in singles and coincidences modes) that were used for the calculation of the new thermonuclear reaction rate. All results are reported in eV, and the statistical and systematic uncertainties are presented separately. The adopted value for the 876 keV resonance strength is the weighted average of our singles measurement and the one from Hardie *et al.* [31]. See the text for details.

E_r (keV)	Literature	Singles	Coincidences	Adopted
561	0.331(41)	···	···	0.331(41)
876	3.80(57)	$3.00^{+0.81}_{-0.72}(\text{stat.}) \pm 0.61(\text{syst.})$	$3.91^{+1.29}_{-1.10}(\text{stat.}) \pm 1.18(\text{syst.})$	3.61(50)
1110	···	$0.125^{+0.027}_{-0.025}(\text{stat.}) \pm 0.015(\text{syst.})$	$0.161^{+0.043}_{-0.041}(\text{stat.}) \pm 0.024(\text{syst.})$	0.125(31)
1155	···	$1.73 \pm 0.25(\text{stat.}) \pm 0.40(\text{syst.})$	$1.79 \pm 0.33(\text{stat.}) \pm 0.42(\text{syst.})$	1.73(47)

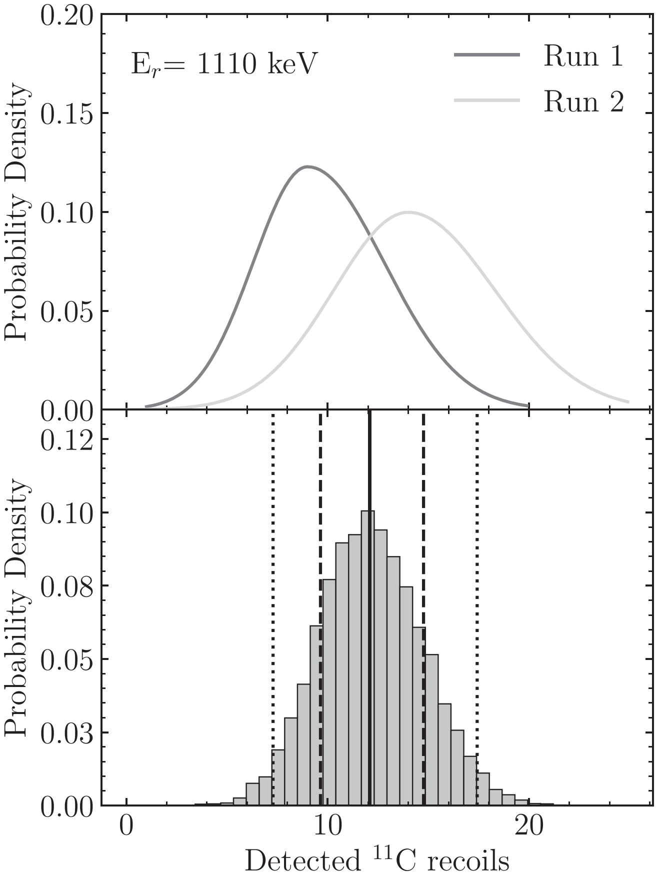

FIG. 9. (Top) Individual probability distributions for the detected ^{11}C recoils in singles mode from the two independent measurements of the 1110 keV resonance. (Bottom) Combined probability distribution from the same measurements. The solid line shows the central value, whereas the dashed and dot lines show the 1 and 2σ uncertainties, respectively. See the text for details.

by DRAGON.[4] Nevertheless, one can see a clear signal in the PID plots (see Figs. 4 and 5). We detected $13^{+4.3}_{-3.7}$ ^{11}C recoil events corresponding to $^{+33.1}_{-28.5}$% 1σ statistical uncertainty, following the Feldman and Cousins [62] prescription for a Poissonian signal with zero background.

Our final result for its strength from the singles analysis is $\omega\gamma_{876} = 3.00^{+0.81}_{-0.72}(\text{stat.}) \pm 0.61(\text{syst.})$ eV. We calculated the weighted average of our measurement and the value by Hardie *et al.* [31] to get the adopted resonance strength $\omega\gamma_{876} =$ 3.61(50) eV, which will be used for the calculation of the thermonuclear reaction rate in Sec. V E. It is worth noting that for all resonances the results for the strength $\omega\gamma$ agree both in coincidence and in singles analysis modes.

Also, from a nuclear structure standpoint, our results for the two previously unknown resonance strengths are in very good agreement with their ^{7}Li$(\alpha,\gamma)^{11}$B analogs [34], namely, $E_x = 9.182$ ($7/2^+$) and 9.271 MeV ($5/2^+$), as they are shown in Table VII. The $5/2^-$ state $E_x = 8.921$ in ^{11}B is the only exception where its resonance strength differs more than two orders of magnitude to its ^{11}C analog.

TABLE VII. Comparison of resonance strengths $\omega\gamma$ for analog states in ^{7}Be$(\alpha,\gamma)^{11}$C and ^{7}Li$(\alpha,\gamma)^{11}$B reactions. Literature data were taken from Kelley *et al.* [34].

J^π	Nucleus	E_x(MeV)	$\omega\gamma$ (eV)
$5/2^-$	^{11}B	8.921(1)	$(8.8 \pm 1.4) \times 10^{-3}$
$5/2^-$	^{11}C	8.420(2)	3.61(50)
$7/2^+$	^{11}B	9.182(2)	0.303(26)
$7/2^+$	^{11}C	8.654(4)	0.125(31)
$5/2^+$	^{11}B	9.271(2)	1.72(24)
$5/2^+$	^{11}C	8.699(2)	1.73(47)

D. Uncertainties

The uncertainties of the final results of the resonance strengths of this paper are of systematic and statistical nature. The former are dominated by the efficiencies of the BGO array (η_{BGO}) and the recoil transmission through the separator ($\eta_{\text{separator}}$), which are inferred from GEANT simulations (Sec. IV F) [42]. Other sources of systematic uncertainty are the MCP detection efficiency, the stopping power measurements, and the charge state fractions.

Furthermore, the statistical uncertainties are due to the low recoil detection yield, caused by the very low transmission of the recoils through the separator, but this parameter is well understood and quantified. As we already pointed out for the 1110- and 876-keV resonances, we used the prescription of Feldman and Cousins [62] for Poissonian signals in zero background to extract the statistical uncertainties.

Table VIII shows a detailed breakdown of the uncertainties for each of the three resonances we measured in the present paper. Note that for the 1110-keV resonance the uncertainty of the average final result was calculated using the procedure discussed in Sec. V B.

E. Thermonuclear reaction rate

The new ^{7}Be$(\alpha,\gamma)^{11}$C thermonuclear reaction rate was calculated using the RatesMC [65] code [66]. Within the RatesMC framework, each nuclear physics input quantity (e.g., resonance energy and resonance strength) has an assigned PDF. The code samples these functions randomly many times ($> 10^3$) using a Monte Carlo algorithm and outputs reaction rates and associated rate probability densities. According to the central limit theorem, a random variable that is determined by the product of many factors will be distributed according to a lognormal density function [66–68]. Using a lognormal PDF, the "low," "recommended," and high Monte Carlo rates are the 16th, 50th (median), and 84th percentile, respectively, of the cumulative reaction rate distribution. In Table IX we present the adopted thermonuclear reaction rate for ^{7}Be$(\alpha,\gamma)^{11}$C.

For our calculation, we used resonance parameters as reported in Kelley *et al.* [34]. More specifically, we included

---

[4] The previous largest maximum recoil angle was $\theta_{r,\max}$= 33 mrad in the study of the ^{12}C$(^{16}$O$,\gamma)^{28}$Si reaction [64].

TABLE VIII. Values given with uncertainties for the quantities used to calculate the resonance strengths in singles and coincidences modes. The relative errors are quoted in parentheses.

Source	1155 keV	1110 keV (Run 1)	1110 keV (Run 2)	876 keV
Detected recoils, $N_{\mathrm{rec}}^{\mathrm{singles}}$	49(7) (14.3%)	$14^{+4.3}_{-3.7}$ ($^{+31}_{-26}$%)	$9^{+3.8}_{-2.7}$ ($^{+42}_{-30}$%)	$16^{+4.3}_{-3.8}$ ($^{+27}_{-24}$%)
Detected recoils, $N_{\mathrm{rec}}^{\mathrm{coinc}}$	33(6) (18.2%)	$9^{+3.8}_{-2.7}$ ($^{+42}_{-30}$%)	$7^{+3.3}_{-2.8}$ ($^{+47}_{-40}$%)	$13^{+4.3}_{-3.7}$ ($^{+33}_{-28}$%)
Charge state fraction, f_q	0.40(1) (2.5%)	0.41(1) (2.4%)	0.41(1) (2.4%)	0.41(1) (2.4%)
Beam particles, $N_{\mathrm{beam}} \times 10^{13}$	1.07(2) (1.9%)	1.76(5) (2.8%)	1.53(5) (3.2%)	2.12(3) (1.41%)
BGO efficiency, η_{BGO}	0.77(1) (1.3%)	0.81(7) (8.6%)	0.81(7) (8.6%)	0.80(18)(22.5%)
Separator transmission, $\eta_{\mathrm{separator}}$	0.141(28) (19.9%)	0.266(18) (6.8%)	0.266(18) (6.8%)	0.016(3) (18.8%)
MCP efficiency[a], η_{MCP}	0.545(59) (10.8%)	0.650(61) (9.4%)	0.321(25) (7.8%)	0.351(19) (5.4%)
Live time, $\eta_{\mathrm{live}}^{\mathrm{singles}}$	0.95409(5) (0.005%)	0.95777(5) (0.005%)	0.99099(5) (0.005%)	0.93408(5) (0.005%)
Live time, $\eta_{\mathrm{live}}^{\mathrm{coinc}}$	0.80381(4) (0.005%)	0.80434(4) (0.005%)	0.82156(4) (0.005%)	0.81571 (0.005%)
Stopping power, ϵ (eV/(10^{15}/cm^2))	40.7(15) (3.7%)	39.7(15) (3.8%)	39.5(15) (3.8%)	41.5(18) (4.3%)
Beam energy (A keV)	462.2(3) (0.06%)	442.6(2) (0.05%)	441.8(2) (0.05%)	351.8(3) (0.09%)
Total uncertainty in singles	14.3% (stat.)	$^{+31}_{-26}$% (stat.)	$^{+42}_{-30}$% (stat.)	$^{+27}_{-24}$% (stat.)
(statistical and systematic)	23.2% (syst.)	12.8% (syst.)	11.8% (syst.)	20.2% (syst.)
Total uncertainty in coincidences	18.2% (stat.)	$^{+42}_{-30}$% (stat.)	$^{+47}_{-40}$% (stat.)	$^{+33}_{-28}$% (stat.)
(statistical and systematic)	23.2% (syst.)	15.4% (syst.)	14.6% (syst.)	30.3% (syst.)

[a] The MCP efficiency includes both the detection efficiency of the system and also the transmission of the recoils through the thin carbon foil that creates the secondary electrons that the MCP detects.

the contribution of the subthreshold resonance at $E_x = 7.4997$ MeV ($E_r = -43.9$ keV) using a γ partial width from the mirror state in ^{11}B [$\Gamma_\gamma = 1.14(4)$ eV] and assumed a reduced α width of 1. According to Descouvemont [37] this resonance can dominate the reaction rate for $T < 0.3$ GK, which can affect the evolution of Population III stars via the hot *pp* chains [20] and the production of ^{7}Li in classical novas [38]. In addition to the narrow resonances at 561, 876, 1110, and 1155 keV, we also included contributions from the broad resonances at 2101, 2236, 2426, and 2539 keV (see Table I for details). For the γ partial widths of the latter states since we used values from the mirror analog ^{11}B, we assigned them a factor of 2 uncertainty.

The new reaction rate uncertainty has been decreased to $\approx$9.4–10.7% over $T =$ 1.5–3 GK, the relevant temperature window for νp-process nucleosynthesis, compared to factors of 1.76–1.91 of the NACRE-II compilation. Although our new rate includes the new measurements of the 1110 and 1155 keV resonance strengths and the updated adopted value for $\omega\gamma_{876}$, it is worth noting that this decrease in the thermonuclear reaction rate is mainly caused from using a Monte Carlo error propagation of the relevant quantities (e.g., E_r, $\omega\gamma$, etc.) [66], and not by the individual contribution of the previously unmeasured resonance strengths. In Fig. 10 we compare the new thermonuclear reaction rate to the NACRE rate [28,36] and an older reaction rate compilation from Caughlan and Fowler [27] (CF88).

Figure 11 shows the individual resonant contributions to the total ^{7}Be$(\alpha,\gamma)^{11}$C reaction rate. For temperatures $T \lessapprox 0.2$ GK, the subthreshold resonance at -43.9 keV dominates the reaction rate, whereas for 0.2 GK $< T <$ 1.0 GK the 561-keV contributes the most since $\Gamma_\alpha \gg \Gamma_\gamma$ (see Table I) and it is the lowest-lying energy resonance [see the discussion in Ref. [69]. For the temperatures relevant for the νp process, 876 keV has a $\approx$60% contribution to the total rate, followed by the 561 keV with $\approx$30%. The 1155-keV resonance has a $\lessapprox$10% contribution, whereas the 1110 keV contributes negligibly to the total reaction rate.

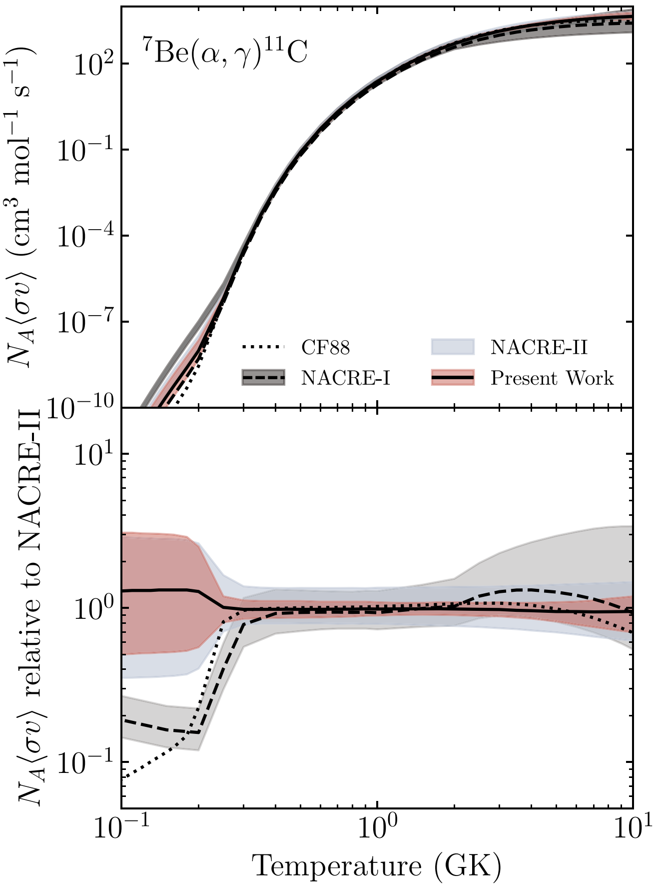

FIG. 10. The new ^{7}Be$(\alpha,\gamma)^{11}$C reaction rate for $T =$ 0.1–10 GK compared to the rates by Refs. [27,28,36] over the same temperature region.

TABLE IX. Total thermonuclear reaction rates for ^{7}Be$(\alpha,\gamma)\,^{11}$C. The rate below $T < 0.012$ GK is zero. The rates are expressed in units of cm^3 mol^{-1} s^{-1}. Columns 2–4 list the 16th, 50th, and 86th percentiles of the total rate PDF at given temperatures. "f.u." is the factor uncertainty, and is obtained from the 16th and 84th percentiles.

T (GK)	Low	Median	High	f.u.
0.012	3.463×10^{-34}	8.835×10^{-34}	2.348×10^{-33}	2.590
0.013	4.535×10^{-33}	1.153×10^{-32}	3.066×10^{-32}	2.588
0.014	4.594×10^{-32}	1.168×10^{-31}	3.097×10^{-31}	2.586
0.015	3.758×10^{-31}	9.552×10^{-31}	2.528×10^{-30}	2.584
0.016	2.563×10^{-30}	6.511×10^{-30}	1.725×10^{-29}	2.583
0.018	7.618×10^{-29}	1.935×10^{-28}	5.129×10^{-28}	2.579
0.020	1.407×10^{-27}	3.572×10^{-27}	9.463×10^{-27}	2.576
0.025	4.793×10^{-25}	1.208×10^{-24}	3.195×10^{-24}	2.568
0.030	4.012×10^{-23}	1.008×10^{-22}	2.665×10^{-22}	2.560
0.040	2.466×10^{-20}	6.147×10^{-20}	1.616×10^{-19}	2.544
0.050	2.309×10^{-18}	5.693×10^{-18}	1.495×10^{-17}	2.528
0.060	7.225×10^{-17}	1.766×10^{-16}	4.628×10^{-16}	2.513
0.070	1.117×10^{-15}	2.705×10^{-15}	7.081×10^{-15}	2.498
0.080	1.057×10^{-14}	2.548×10^{-14}	6.647×10^{-14}	2.483
0.090	6.993×10^{-14}	1.681×10^{-13}	4.372×10^{-13}	2.468
0.100	3.570×10^{-13}	8.501×10^{-13}	2.201×10^{-12}	2.453
0.110	1.472×10^{-12}	3.490×10^{-12}	8.984×10^{-12}	2.439
0.120	5.172×10^{-12}	1.216×10^{-11}	3.106×10^{-11}	2.424
0.130	1.580×10^{-11}	3.679×10^{-11}	9.412×10^{-11}	2.410
0.140	4.322×10^{-11}	9.999×10^{-11}	2.548×10^{-10}	2.396
0.150	1.078×10^{-10}	2.473×10^{-10}	6.275×10^{-10}	2.382
0.160	2.482×10^{-10}	5.656×10^{-10}	1.429×10^{-9}	2.367
0.180	1.116×10^{-9}	2.459×10^{-9}	6.115×10^{-9}	2.310
0.200	4.918×10^{-9}	9.604×10^{-9}	2.208×10^{-8}	2.096
0.250	5.348×10^{-7}	6.305×10^{-7}	7.894×10^{-7}	1.251
0.300	2.666×10^{-5}	3.051×10^{-5}	3.506×10^{-5}	1.147
0.350	4.586×10^{-4}	5.215×10^{-4}	5.955×10^{-4}	1.142
0.400	3.813×10^{-3}	4.334×10^{-3}	4.923×10^{-3}	1.139
0.450	1.950×10^{-2}	2.209×10^{-2}	2.507×10^{-2}	1.137
0.500	7.106×10^{-2}	8.022×10^{-2}	9.077×10^{-2}	1.135
0.600	4.816×10^{-1}	5.413×10^{-1}	6.105×10^{-1}	1.130
0.700	1.860×10^{0}	2.083×10^{0}	2.340×10^{0}	1.125
0.800	5.136×10^{0}	5.726×10^{0}	6.390×10^{0}	1.118
0.900	1.139×10^{1}	1.265×10^{1}	1.401×10^{1}	1.111
1.000	2.178×10^{1}	2.407×10^{1}	2.651×10^{1}	1.105
1.250	7.217×10^{1}	7.907×10^{1}	8.638×10^{1}	1.095
1.500	1.633×10^{2}	1.792×10^{2}	1.953×10^{2}	1.094
1.750	2.946×10^{2}	3.236×10^{2}	3.538×10^{2}	1.095
2.000	4.578×10^{2}	5.041×10^{2}	5.522×10^{2}	1.098
2.500	8.379×10^{2}	9.262×10^{2}	1.021×10^{3}	1.103
3.000	1.235×10^{3}	1.370×10^{3}	1.516×10^{3}	1.107
3.500	1.612×10^{3}	1.801×10^{3}	2.003×10^{3}	1.116
4.000	1.955×10^{3}	2.195×10^{3}	2.468×10^{3}	1.129
5.000	2.515×10^{3}	2.876×10^{3}	3.332×10^{3}	1.167
6.000	2.924×10^{3}	3.398×10^{3}	4.121×10^{3}	1.210
7.000	3.202×10^{3}	3.812×10^{3}	4.777×10^{3}	1.250
8.000	3.386×10^{3}	4.112×10^{3}	5.325×10^{3}	1.284
9.000	3.503×10^{3}	4.324×10^{3}	5.765×10^{3}	1.312
10.000	3.558×10^{3}	4.460×10^{3}	6.079×10^{3}	1.335

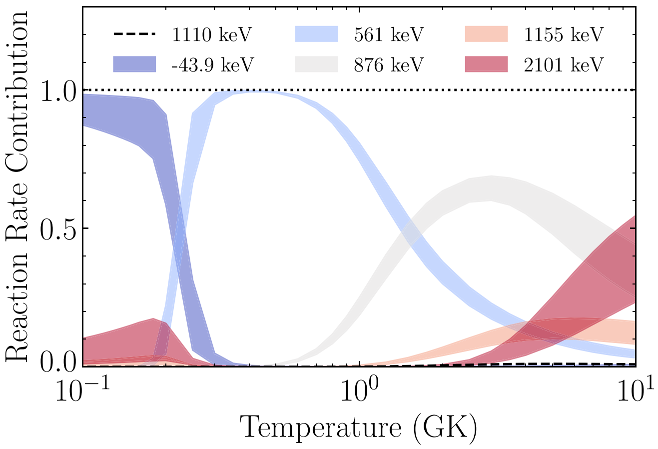

FIG. 11. Resonant contributions to the ^{7}Be$(\alpha,\gamma)^{11}$C thermonuclear reaction rate. The dotted line at the bottom right corner shows the contribution of the 1110-keV resonance.

The effect of the new reaction rate will be studied extensively in a future publication, taking into account new measurements of the ^{10}B$(\alpha,p)^{13}$C reaction [70], which was also included in the sensitivity study of Wanajo *et al.* [22], and the ^{59}Cu$(p,\alpha)^{56}$Ni [71] which may be responsible for the Ni-Cu cycle [23].

In addition to the thermonuclear reaction rate, we also calculated the astrophysical S factor. In Fig. 12 we present the astrophysical S factor for ^{7}Be$(\alpha,\gamma)^{11}$C with the individual resonant contributions. Our results agree well with the NACRE-II data with the exception of the 2101-keV resonance which seems to be misplaced to lower energies [see Fig. 42 in Ref. [36]].

VI. DISCUSSION AND CONCLUSIONS

In the present paper we performed the first inverse kinematics study of the ^{7}Be$(\alpha,\gamma)^{11}$C reaction to measure unknown resonance strengths at energies relevant to νp-process

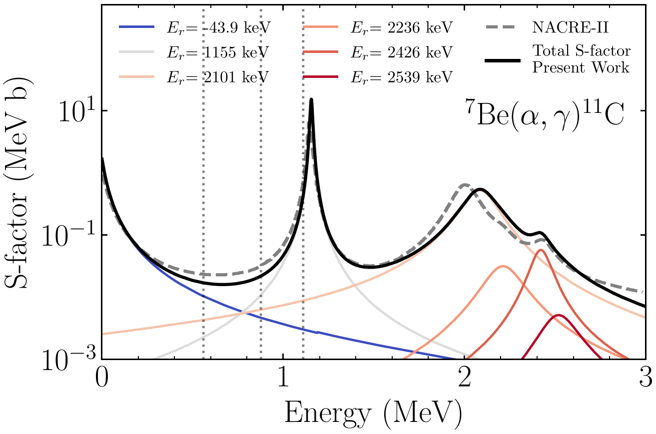

FIG. 12. The astrophysical S factor for the ^{7}Be$(\alpha,\gamma)^{11}$C reaction based on our RatesMC calculations. Contributions from different resonances are shown. The narrow resonances at 561, 876, and 1110 keV are shown with the vertical dotted lines. The astrophysical S factor from NACRE-II [36] is also shown.

nucleosynthesis. We report the first measurement of the 1155- and 1110-keV resonances with strengths of $1.73 \pm 0.25(\text{stat.}) \pm 0.40(\text{syst.})$ eV and $125^{+27}_{-25}(\text{stat.}) \pm 15(\text{syst.})$ MeV, respectively. We also remeasured the 876-keV resonance strength ($\omega\gamma_{876} = 3.00^{+0.81}_{-0.72}(\text{stat.}) \pm 0.61(\text{syst.})$ eV) and our result agrees with the measurement of Hardie *et al.* [31] [$\omega\gamma = 3.80(57)$ eV].

As we have also demonstrated in Psaltis *et al.* [47], the present paper shows that DRAGON is capable of handling measurements in which the maximum recoil cone angle exceeds its acceptance after a systematic study of the BGO array efficiency and its transmission using extensive GEANT simulations. That opens a new avenue for future experiments using DRAGON, that were previously thought to be inaccessible due to large maximum recoil angles (e.g., $^{18}\text{O}(\alpha,\gamma)^{22}\text{Ne}$, $^{20}\text{Ne}(\alpha,\gamma)^{24}\text{Mg}$ and others).

The new $^{7}\text{Be}(\alpha,\gamma)^{11}\text{C}$ reaction rate is constrained to 9.4–10.7% for $T = 1.5$–3 GK which is sufficient for nucleosynthesis calculations. The effect of the rate, along with other measured reactions relevant to nucleosynthesis in neutrino-driven winds will be explored in a subsequent study. According to the work of Wanajo *et al.* [22], the $^{7}\text{Be}(\alpha,\gamma)^{11}\text{C}$ reaction rate in the relevant energies can affect the number of the neutron-to-seed ratio Δ_n, regulating the νp-process efficiency in synthesizing neutron-deficient isotopes. This is a particularly interesting result since most recent self-consistent three-dimensional core-collapse supernova simulations favor proton-rich conditions [72]. In addition, a rigorous study of the astrophysical conditions of the proton-rich neutrino driven ejecta, and how they produce different nucleosynthesis outputs, using all the up-to-date nuclear physics input is desired.

The intense ^{7}Be ion-beam facilities produced with carbide targets can be utilized for more demanding experiments, such as $^{7}\text{Be}(p,\gamma)$ and ^{7}Be α scattering. Pure graphite targets bombarded by protons at 100 μA (or a UC_x target at 40 μA) could produce as much as 10^{10} s^{-1} of ^{7}Be.

ACKNOWLEDGMENTS

We gratefully acknowledge the beam delivery and ISAC operations groups at TRIUMF. In particular, we thank F. Ames, T. Angus, A. Gottberg, S. Kiy, J. Lassen, and O. Shelbaya for all their help during the experiment. We thank the anonymous referee for useful comments that improved the paper. The core operations of TRIUMF are supported via a contribution from the federal government through the National Research Council of Canada, and the Government of British Columbia provides building capital funds. Authors from McMaster University are funded by the National Sciences and Engineering Research Council of Canada (NSERC). DRAGON is funded through NSERC Grant No. SAPPJ-2019-00039. A.P. also acknowledges support from the Deutsche Forschungsgemeinschaft (DFG, German Research Foundation Project No. 279384907-SFB 1245, and the State of Hesse within the Research Cluster ELEMENTS (Project No. 500/10.006). R.L. and C.M. acknowledge support from the U.S. Department of Energy, Office of Science, Office of Nuclear Physics under Grants No. DE-SC0017799 and No. DE-FG02-97ER41042. C.R.B., R.G., and S.P. acknowledge support from the U.S. Department of Energy, under Grants No. DE-FG02-88ER40387 and No. DE-NA0003883. Authors from Colorado School of Mines acknowledge support from U.S. Department of Energy Office of Science DE-FG02-93ER40789 grant. Authors from the UK are supported by the Science and Technology Facilities Council (STFC). This work benefited from discussions at the "Nuclear Astrophysics at Rings and Recoil Separators" Workshop supported by the National Science Foundation under Grant No. PHY-1430152 (JINA Center for the Evolution of the Elements).

[1] M. Arnould and S. Goriely, Phys. Rep. **384**, 1 (2003).
[2] T. Rauscher *et al.*, Rep. Prog. Phys. **76**, 066201 (2013).
[3] M. Pignatari *et al.*, Int. J. Mod. Phys. E **25**, 1630003 (2016).
[4] A. G. W. Cameron, Publ. Astron. Soc. Pac. **69**, 201 (1957).
[5] K. Lodders, H. Palme, and H.-P. Gail, 4.4 Abundances of the elements in the Solar System, in *Solar System*, edited by J. E. Trümper, Landolt-Brnstein - Group VI Astronomy and Astrophysics, Vol. 4B (Springer-Verlag, Berlin Heidelberg, 2009), pp. 560–630.
[6] C. Travaglio *et al.*, Astrophys. J. **795**, 141 (2014).
[7] H. Schatz *et al.*, Phys. Rep. **294**, 167 (1998).
[8] W. Rapp *et al.*, Astrophys. J. **653**, 474 (2006).
[9] T. Rauscher *et al.*, Mon. Not. R. Astron. Soc. **463**, 4153 (2016).
[10] L. Hüdepohl, B. Müller, H.-T. Janka, A. Marek, and G. G. Raffelt, Phys. Rev. Lett. **104**, 251101 (2010).
[11] T. Fischer *et al.*, Astron. Astrophys. **517**, A80 (2010).
[12] O. Just *et al.*, Mon. Not. R. Astron. Soc. **453**, 3387 (2015).
[13] E. O'Connor, Astrophys. J., Suppl. Series **219**, 24 (2015).
[14] A. Arcones and F. Montes, Astrophys. J. **731**, 5 (2011).
[15] S. Wanajo *et al.*, Astrophys. J. **852**, 40 (2018).
[16] D. Vartanyan *et al.*, Mon. Not. R. Astron. Soc. **482**, 351 (2019).
[17] C. Fröhlich, G. Martínez-Pinedo, M. Liebendörfer, F.-K. Thielemann, E. Bravo, W. R. Hix, K. Langanke, and N. T. Zinner, Phys. Rev. Lett. **96**, 142502 (2006).
[18] S. Wanajo, Astrophys. J. **647**, 1323 (2006).
[19] J. Pruet *et al.*, Astrophys. J. **644**, 1028 (2006).
[20] M. Wiescher *et al.*, Astrophys. J. **343**, 352 (1989).
[21] J. José and C. Iliadis, Rep. Prog. Phys. **74**, 096901 (2011).
[22] S. Wanajo *et al.*, Astrophys. J. **729**, 46 (2011).
[23] A. Arcones, C. Fröhlich, and G. Martínez-Pinedo, Astrophys. J. **750**, 18 (2012).
[24] C. Fröhlich and T. Rauscher, in *Origin of Matter and Evolution of Galaxies 2011*, edited by S. Kubono, T. Hayakewa, T. Kajino, H. Miyatake, T. Motobayashi, and K. Nomoto, AIP Conf. Proc. No. 1484 (AIPs, Melville, NY, 2012), pp. 232–239.
[25] M. Jacobi, Influence of astrophysical and nuclear physics uncertainties on the nucleosynthesis in proton-rich neutrino-driven winds, Master's thesis, Technische Universität Darmstadt, 2018.

[26] N Nishimura *et al.*, Mon. Not. R. Astron. Soc. **489**, 1379 (2019).
[27] G. R. Caughlan and W. A. Fowler, At. Data Nucl. Data Tables **40**, 283 (1988).
[28] C. Angulo *et al.*, Nucl. Phys. A **656**, 3 (1999).
[29] H. O. Fynbo *et al.*, Nature (London) **433**, 136 (2005).
[30] S. Jin *et al.*, Nature (London) **588**, 57 (2020).
[31] G. Hardie, B. W. Filippone, A. J. Elwyn, M. Wiescher, and R. E. Segel, Phys. Rev. C **29**, 1199 (1984).
[32] M. Wiescher *et al.*, Phys. Rev. C **28**, 1431 (1983).
[33] H. Yamaguchi *et al.*, Phys. Rev. C **87**, 034303 (2013).
[34] J. Kelley *et al.*, Nucl. Phys. A **880**, 88 (2012).
[35] Y. Yanagisawa *et al.*, Nucl. Instrum. Methods Phys. Res., Sect. A **539**, 74 (2005).
[36] Y. Xu *et al.*, Nucl. Phys. A **918**, 61 (2013).
[37] P. Descouvemont, Nucl. Phys. A **584**, 532 (1995).
[38] M. Hernanz, J. José, A. Coc, and J. Isern, Astrophys. J. Lett. **465**, L27 (1996).
[39] D. Hutcheon *et al.*, Nucl. Instrum. Methods Phys. Res., Sect. A **498**, 190 (2003).
[40] J. Lassen *et al.*, Hyperfine Interact. **162**, 69 (2006).
[41] M. Gaelens *et al.*, Nucl. Instrum. Methods Phys. Res., Sect. B **204**, 48 (2003).
[42] C. Ruiz *et al.*, Eur. Phys. J. A **50**, 99 (2014).
[43] C. Vockenhuber *et al.*, Nucl. Instrum. Methods Phys. Res., Sect. A **603**, 372 (2009).
[44] G. Christian *et al.*, Eur. Phys. J. A **50**, 75 (2014).
[45] D. G. Gigliotti *et al.*, Nucl. Instrum. Methods Phys. Res., Sect. B **204**, 671 (2003).
[46] D. G. Gigliotti, Efficiency calibration measurement and GEANT simulation of the DRAGON BGO gamma ray array at TRIUMF, Master's thesis, University of Northern British Columbia, Prince George, Canada, 2004.
[47] A. Psaltis *et al.*, Nucl. Instrum. Methods Phys. Res., Sect. A **987**, 164828 (2021).
[48] A. Psaltis, Radiative alpha capture on ^{7}Be with DRAGON at νp–process nucleosynthesis energies, Ph.D. thesis, McMaster University, 2020.
[49] W. A. Fowler *et al.*, Rev. Mod. Phys. **20**, 236 (1948).
[50] S. Sjue *et al.*, Nucl. Instrum. Methods Phys. Res., Sect. A **700**, 179 (2013).
[51] U. Hager *et al.*, Phys. Rev. C **85**, 035803 (2012).
[52] D. Connolly *et al.*, Phys. Rev. C **97**, 035801 (2018).
[53] M. Williams *et al.*, Phys. Rev. C **102**, 035801 (2020).
[54] J. M. D'Auria *et al.*, Phys. Rev. C **69**, 065803 (2004).
[55] K. Jayamanna, Hyperfine Interact. **225**, 51 (2014).
[56] W. Liu *et al.*, Nucl. Instrum. Methods Phys. Res., Sect. A **496**, 198 (2003).
[57] J. F. Ziegler *et al.*, Nucl. Instrum. Methods Phys. Res., Sect. B **268**, 1818 (2010).
[58] The GEANT simulation package of DRAGON can be found in https://github.com/DRAGON-Collaboration/G3_DRAGON.
[59] C. Matei *et al.*, Phys. Rev. Lett. **97**, 242503 (2006).
[60] H. Rose and D. Brink, Rev. Mod. Phys. **39**, 306 (1967).
[61] A. Psaltis *et al.*, Phys. Rev. Lett. **129**, 162701 (2022).
[62] G. J. Feldman and R. D. Cousins, Phys. Rev. D **57**, 3873 (1998).
[63] K. F. Wallis, Stat. Sci. **29**, 106 (2014).
[64] D. Lebhertz *et al.*, Phys. Rev. C **85**, 034333 (2012).
[65] The RatesMC code to calculate thermonuclear reaction rates can be found in https://github.com/rlongland/RatesMC.
[66] R. Longland *et al.*, Nucl. Phys. A **841**, 1 (2010).
[67] J. H. Gaddum, Nature (London) **156**, 463 (1945).
[68] C. Iliadis *et al.*, J. Phys. G: Nucl. Part. Phys. **42**, 034007 (2015).
[69] C. Iliadis, *Nuclear Physics of Stars* (John Wiley & Sons, Hoboken, NJ, 2015).
[70] Q. Liu *et al.*, Phys. Rev. C **101**, 025808 (2020).
[71] J. S. Randhawa *et al.*, Phys. Rev. C **104**, L042801 (2021).
[72] R. Bollig *et al.*, Astrophys. J. **915**, 28 (2021).